

OPEN

Evaluating the potential of hyperpolarised [1-¹³C] L-lactate as a neuroprotectant metabolic biosensor for stroke

Jean-Noël Hyacinthe ^{1,2,6}, Lara Buscemi ^{3,6}, Thanh Phong Lê ^{1,4}, Mario Lepore⁵, Lorenz Hirt ³ & Mor Mishkovsky ^{4*}

Cerebral metabolism, which can be monitored by magnetic resonance spectroscopy (MRS), changes rapidly after brain ischaemic injury. Hyperpolarisation techniques boost ¹³C MRS sensitivity by several orders of magnitude, thereby enabling *in vivo* monitoring of biochemical transformations of hyperpolarised (HP) ¹³C-labelled precursors with a time resolution of seconds. The exogenous administration of the metabolite L-lactate was shown to decrease lesion size and ameliorate neurological outcome in preclinical studies in rodent stroke models, as well as influencing brain metabolism in clinical pilot studies of acute brain injury patients. The aim of this study was to demonstrate the feasibility of measuring HP [1-¹³C] L-lactate metabolism in real-time in the mouse brain after ischaemic stroke when administered after reperfusion at a therapeutic dose. We showed a rapid, time-after-reperfusion-dependent conversion of [1-¹³C] L-lactate to [1-¹³C] pyruvate and [¹³C] bicarbonate that brings new insights into the neuroprotection mechanism of L-lactate. Moreover, this study paves the way for the use of HP [1-¹³C] L-lactate as a sensitive molecular-imaging biosensor in ischaemic stroke patients after endovascular clot removal.

Stroke is the second most common cause of death and the third leading cause of disability worldwide¹. Approximately 85% of strokes are of the ischaemic subtype that can be treated by restoring blood flow to the ischaemic brain through thrombolysis or thrombectomy within a relatively narrow time window of 4.5–7.3 hours after ischemic onset^{2–4}. Interestingly, the evolution of ischaemic damage can vary between patients and careful patient selection based on imaging properties of the ischaemic brain allows performing thrombolysis up to 9 hours after ischemia onset and thrombectomy up to 24 hours with a significant improvement in the outcome⁵.

Thanks to recent advances⁵, the number of stroke patients receiving treatment increased in the past years (now about 15–20% in Switzerland), but even for treated patients good outcome is not guaranteed. In addition to timely clot-removal interventions, neuroprotective strategies applied in the acute phase of ischaemic stroke could improve patient outcome by enhancing the recovery of brain cells not yet irreversibly damaged or by promoting the brain's endogenous self-repair mechanisms. Nonetheless, despite the many different neuroprotective approaches proposed from preclinical results, so far none were shown to be effective at a clinical level^{6,7}.

It is well established that large amounts of the metabolite lactate are produced in brain areas subjected to hypoxia due to reduced blood supply^{8,9}. Once considered an end product of metabolism, increasing evidence supports a role of lactate as an energy substrate for the brain^{10,11} leading to the hypothesis that elevated lactate concentrations after cerebral ischaemia can be used to fuel the brain. Several *in vivo* studies have emphasised the need of lactate to sustain neuronal recovery directly after ischaemia^{12–14}. Interestingly, it has been shown that exogenous lactate administration after transient cerebral ischaemia at reperfusion protects against ischemia-induced cell

¹Geneva School of Health Sciences, HES-SO University of Applied Sciences and Arts Western Switzerland, Geneva, Switzerland. ²Image Guided Intervention Laboratory, Faculty of Medicine, University of Geneva, Geneva, Switzerland. ³Department of Clinical Neurosciences, Centre Hospitalier Universitaire Vaudois, Lausanne, Switzerland. ⁴Laboratory of Functional and Metabolic Imaging, École polytechnique fédérale de Lausanne (EPFL), Lausanne, Switzerland. ⁵Centre d'Imagerie Biomédicale (CIBM), École polytechnique fédérale de Lausanne (EPFL), Lausanne, Switzerland. ⁶These authors contributed equally: Jean-Noël Hyacinthe and Lara Buscemi. *email: mor.mishkovsky@epfl.ch

death and disability^{15,16}. A dual mode of action was suggested for lactate to provide neuroprotection by constituting an energy substrate transported by monocarboxylate transporters (MCTs) to deprived neurons, or by signalling via the hydroxycarboxylic acid receptor 1 (HCAR1), thus involving both metabolism and signalling¹⁷. Furthermore, in pilot clinical studies, lactate was safely administered to acute brain injury patients and proved to be beneficial against intracranial hypertension and improved cerebral glucose availability^{18,19}.

Magnetic resonance spectroscopy (MRS) techniques provide tools to study cerebral metabolism non-invasively. The evolution of the neurochemical profile composed of the endogenous molecules detected by ¹H MRS after cerebral ischaemia-reperfusion^{8,9,20,21} illustrates the impact of ischaemia on brain metabolism. MRS can also be used to track metabolism of exogenously infused non-hyperpolarised (i.e. thermally polarised) ¹³C-labelled metabolic tracers using ¹³C MRS, but its low sensitivity limits clinical application. The recent development of hyperpolarised (HP) ¹³C MRS by dissolution dynamic nuclear polarisation (dDNP)²² enables boosting MR sensitivity and monitoring brain metabolism *in vivo* in real time in preclinical studies^{23–27} and clinical settings^{28–30}. In the context of ischaemic stroke, it was recently demonstrated that molecular imaging of HP [^{1-¹³C}] pyruvate could highlight differences between the penumbra and intact remote regions³¹. Lactate is among the many endogenous molecules that can be polarised^{32–36} and given that the plasma concentration of endogenous lactate is rather high, it can be safely administered at the typical millimolar concentrations necessary for both HP ¹³C MRS measurements^{33–36} and neuroprotection¹⁶.

The aim of this study was to demonstrate the feasibility of measuring HP [^{1-¹³C}] lactate metabolism in the mouse brain when administered at a therapeutic dose after ischaemic stroke at different reperfusion time points to evaluate the potential of HP lactate as a theranostic biosensor for stroke. Notably, kinetics of HP lactate metabolism may help to shed light on the puzzling dual mechanism of lactate neuroprotection.

Materials and Methods

Animal experimentation. All experimental procedures involving mice were approved by the regulatory body of the Canton Vaud, Switzerland (Service de la consommation et des affaires vétérinaires) license number VD2017.5, and all experiments were conducted according to Federal and local ethical guidelines and complied with the ARRIVE guidelines. Male C57BL/6J mice (n = 34, 7–9 weeks of age, body weight 25.71 ± 2.14 g, Charles River, France) were given free access to food and water and were maintained in a 12 h light-dark cycle in a temperature- and humidity-controlled animal facility.

Transient middle cerebral artery occlusion (MCAO). Mice were anaesthetised with isoflurane (1.5–2.0% in 60% oxygen) using a facemask. Regional cerebral blood flow (rCBF) was measured throughout the operation by laser-Doppler flowmetry (Perimed AB, Sweden) with a flexible probe fixed on the skull at 1 mm posterior and 6 mm lateral from bregma. Transient focal cerebral ischaemia was induced by occlusion of the left middle cerebral artery (MCA) with an intra-luminal suture as described previously^{17,37}. Briefly, the left common carotid artery and the left external carotid artery were surgically exposed and ligated following a ventral midline neck incision and ischaemia was induced by inserting a silicone-coated nylon monofilament (Doccol Corp, USA) through the common carotid artery into the internal carotid artery. rCBF was maintained below 20% of the baseline for 30 minutes, after which the occluding filament was withdrawn to allow reperfusion. Occlusion was considered successful if rCBF decreased by at least 80% of the start value and reperfusion if the rCBF rose above 50% of baseline within 10 min after filament removal. 5 out of the 34 mice that underwent the surgical procedure were not included in the study, as one did not reach the 80% reduction during occlusion and 4 mice did not reperfuse to 50% of the starting rCBF. Sham operated mice underwent a similar surgical procedure but without MCA occlusion. In order to minimise anaesthesia duration, the femoral vein was catheterised during the 30-minute ischaemia to allow subsequent intravenous (i.v.) HP [^{1-¹³C}] lactate injection.

Hyperpolarisation. HP [^{1-¹³C}] lactate was prepared as previously described³⁴. Briefly, frozen beads containing sodium [^{1-¹³C}] L-lactate solution (45–55% (w/w) in H₂O, Sigma Aldrich) and d₈-glycerol (Sigma Aldrich) were mixed 1:1 (w/w). The sample was dynamically polarised using TEMPOL radical (58 mM, Sigma Aldrich) as polarising agent on a custom-designed 7 T DNP polariser operating at 197 GHz/1.00 ± 0.05 K³⁸ for 2 h, then rapidly dissolved in 5 mL of superheated D₂O and transferred within 2 s into the separator/infusion pump³⁹, which was positioned inside the magnet bore. The [^{1-¹³C}] lactate polarisation measured at the separator was 15.6 ± 2.0% (n = 5). A bolus of the solution was automatically infused over 3 s through the catheterised mouse femoral vein as previously described⁴⁰.

Magnetic resonance measurements. We performed all measurements on a Varian INOVA spectrometer (Varian, Palo Alto, CA, USA) interfaced to a 31 cm horizontal-bore actively shielded 9.4 T magnet (Magnex Scientific, Abingdon, UK).

Hyperpolarised ¹³C MRS. Directly after reperfusion, animals were placed into the MR scanner. We performed ¹³C MR measurements using a home-built ¹H-quadrature/¹³C-single loop surface coil that we placed on top of the mouse's head. The sensitivity profile of the ¹³C-single loop surface coil limits the signal detection to the mouse head. Coil specifications are presented in the Supporting Information (Fig. S1). B₀ inhomogeneity was corrected using the FASTESTMAP algorithm⁴¹. Anatomical T₂ weighted (T_{2w}) images were acquired (fast spin echo imaging) before i.v. bolus infusion of the HP solution (either 325 or 350 μL, 90 mM HP [^{1-¹³C}] lactate solution and a dead volume of either 125 μL or 350 μL respectively, note that in earlier measurements we injected the larger dead volume and then improved our system to reduce it) by the automated protocol⁴⁰. The chosen lactate dose (1.16 mmol/kg) was based on the optimal therapeutic dose used in Berthet *et al.*¹⁶ and resulted in a [^{1-¹³C}] lactate concentration in blood immediately after injection of 12.9 ± 0.9 mM. HP solutions were injected 1 h or 2 h

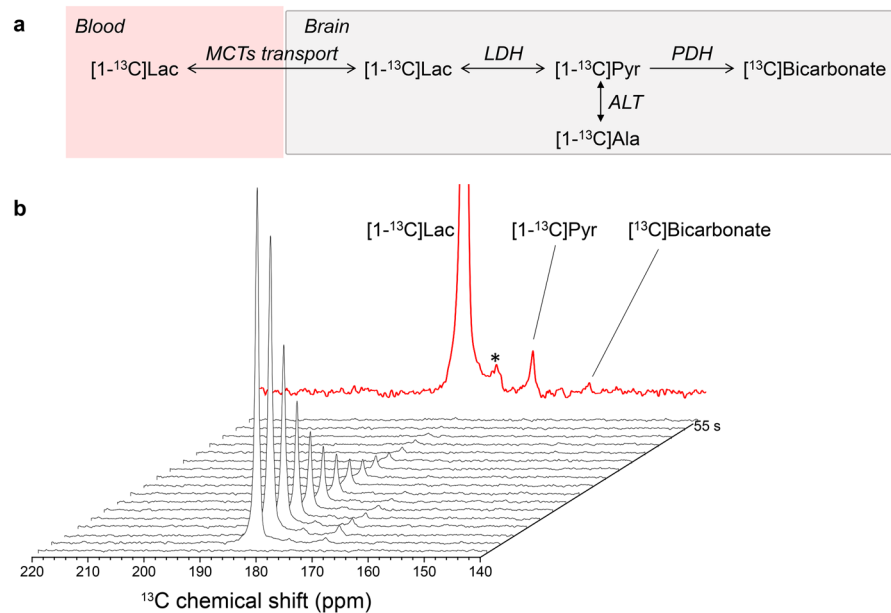


Figure 1. (a) Simplified scheme of the cerebral metabolism of HP [1-¹³C] lactate. (b) Dynamic ¹³C MRS spectra measured in the head of an MCAO mouse following the injection of HP [1-¹³C] lactate (183.5 ppm). The transfer of the label to [1-¹³C] pyruvate at 171.5 ppm can be readily detected. In the sum of the spectra shown in the top panel (red), the peak of ¹³C bicarbonate becomes visible at 161.5 ppm. The peak designated by (*) at 176 ppm results from chemical impurities that overlap with the expected [1-¹³C] alanine peak.

post-reperfusion after MCAO surgery and 1 h post-surgery in sham operated animals ($n = 5$ each, 15 mice in total). A series of pulse-acquire (30°, BIR-4 pulse⁴²) spectra was triggered 1.5 s post-injection and repeated every 3 s for 3 min.

The area under the curve (AUC) of the metabolites was calculated using VNMRJ software by integrating the ¹³C MRS spectra after phase and baseline correction. The peak areas of [1-¹³C] lactate, [1-¹³C] pyruvate, and [¹³C] bicarbonate were quantified, averaged over 10 acquisitions (sum of spectra 3–13, corresponding to a total acquisition time of 37.5 s), and used to compute the pyruvate-to-lactate (PLR) and bicarbonate-to-lactate (BLR) ratios. To reduce the variability between animals, data was corrected by scaling it to the HP [1-¹³C] lactate concentration in blood immediately after the injection, namely by multiplying the number of moles of [1-¹³C] lactate injected (i.e. 90 mM multiplied by either 325 or 350 μ L) and dividing by the animal's blood volume plus the total injected volume resulting in corrected ratios cPLR and cBLR respectively. The blood volume of the individual animal was estimated as 7% of the body weight⁴³.

Proton MRS. Proton spectra were acquired on a different set of animals after MCAO surgery ($n = 3$) and sham operated animals ($n = 3$) both without lactate injection. We performed the measurements using a home-built ¹H-quadrature surface coil located on top of the mouse's head. Quickly after completion of the 30 min MCAO with successful reperfusion, animals were placed carefully into the MR scanner. T_{2W} images were acquired and B_0 inhomogeneity was corrected at the voxel located at the striatum where the lesion is expected to form ($2 \times 1.8 \times 2$ mm³, 7.2 μ L). A series of ¹H MRS spectra were acquired using SPECIAL pulse sequences⁴⁴ (TE/TR = 2.8/4000 ms, 200 ms acquisition time in 10×16 scans) and repeated continuously until about 200 min post-reperfusion. Metabolite concentrations were calculated using LCModel-based fitting routine⁴⁵.

Immunostaining. To assess variation in monocarboxylate transporter (MCT) distribution and expression following 30 min MCAO at the injection time points (i.e. 1 h and 2 h post-reperfusion), we performed immunostaining using MCT1, MCT2 and MCT4 antibodies. Eight male C57BL/6J mice (sham, $n = 2$; 1 h post-reperfusion, $n = 3$; 2 h post-reperfusion, $n = 3$) were used. Note that lactate was not injected in any of these animals. At the set time-points after ischaemia-reperfusion, mice were sacrificed by intraperitoneal injection of 150 mg/kg sodium pentobarbital and intracardially perfused with 4% paraformaldehyde in phosphate buffer at pH 7.4. Dissected brains were post-fixed overnight, cryoprotected in 30% sucrose and cut as 30 μ m cryostat coronal sections. Free-floating sections were blocked in 0.5% casein and then incubated overnight at 4 °C with primary antibodies in 0.1% Triton X-100-PBS-1% BSA, rinsed in PBS and incubated with Alexa Fluor-coupled secondary antibodies (ThermoFisher-Molecular Probes) and DAPI for nuclear counterstaining one hour at room temperature. Slices were finally rinsed in PBS and mounted in FluorSave™ (Calbiochem). The antibodies used were: anti-Microtubule Associated Protein-2 (MAP-2) mouse monoclonal antibody (Millipore #MAB3418, 1:400); anti-Platelet Endothelial Cell Adhesion Molecule-1 (PECAM-1, also known as CD31) rat monoclonal antibody (BD Pharmingen #550274, 1:100); anti-Monocarboxylate Transporter 4 (MCT4) rabbit polyclonal antibody (Santa Cruz Biotechnology #sc-50329, 1:500); anti-Monocarboxylate Transporter 1 (MCT1) and

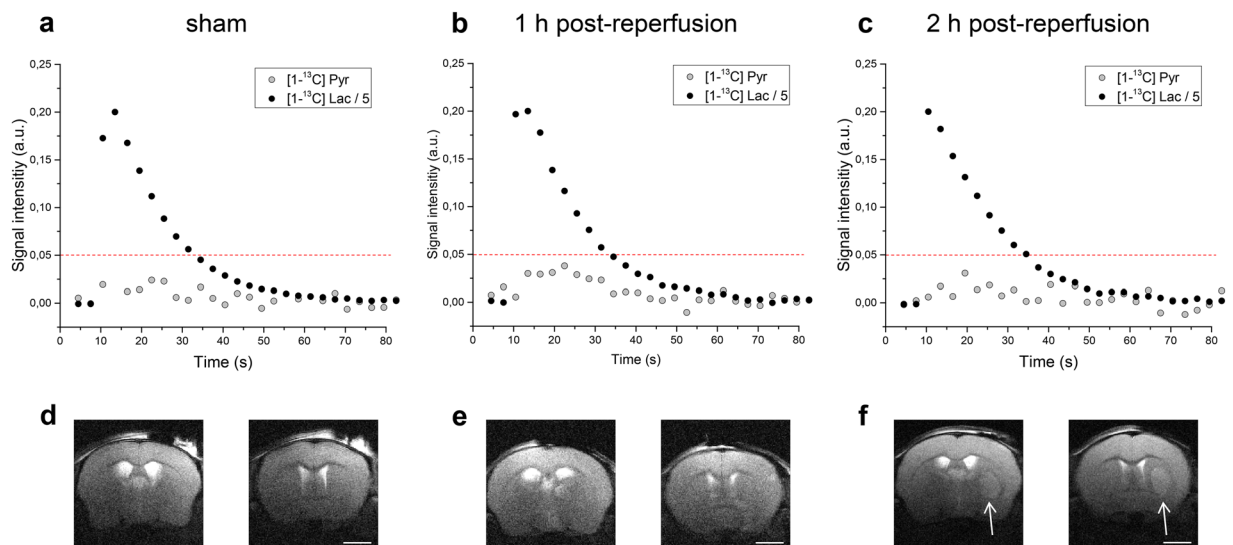


Figure 2. Representative *in vivo* time courses of [$1\text{-}^{13}\text{C}$] lactate (black) and its metabolic product [$1\text{-}^{13}\text{C}$] pyruvate (grey) in the brain of sham operated mice (a) and of mice at different times after ischaemia onset (b,c). Each time course was normalised to the respective maximal lactate signal. The red dotted line was added to highlight the differences in [$1\text{-}^{13}\text{C}$] pyruvate labelling. The corresponding T_{2W} axial images of the brains of sham operated mice (d) and mice at different time points after ischaemia onset (e,f) are presented at the bottom of each time course. While a clear lesion can be detected 2 h post-reperfusion (f, white arrow), the morphological modifications are still obscured at 1 h post-reperfusion (e). Images acquired ca. 5 min before the infusion of HP [$1\text{-}^{13}\text{C}$] lactate, showing two axial slices out of 14 one mm thickness slices. Other experimental parameters: effective echo time and repetition time: $TE_{\text{eff}}/TR = 52/4000$ ms, 2 scans, $18\text{ mm} \times 18\text{ mm}$ FOV with matrix size 256×256 . Scalebar: 2 mm.

anti-Monocarboxylate Transporter 2 (MCT2) rabbit polyclonal antibodies⁴⁶ were both used at a 1:500 dilution and were a kind gift of Prof. Luc Pellerin. Three z-stack images (9–11 images/stack, $z = 1.5\ \mu\text{m}$) per section were acquired with a TCS SP5 RS – DM6000 confocal scanning microscope (Leica, Germany) at 20 x magnification (HC PL Fluotar, NA 0.5, air). Representative confocal images are displayed as maximal z-projections. Images were processed with Fiji/ImageJ software (NIH, USA) and Adobe Photoshop CS5 (Adobe, USA).

Statistical analysis. We performed statistical analyses using the OriginPro 2016 software. One-way analysis of variance (One-way ANOVA) was used followed by Tukey's test. A p value of 0.05 was considered significant. All data are presented as means \pm standard deviation unless otherwise stated. For this feasibility study, we selected the group size based on our previous experience with this model^{15,20,47}. We could not be blind to the measurements due to the imaging methodologies employed. Data can be accessed on request from the corresponding author.

Ethical approval and informed consent. All experimental protocols were approved by the Vaud Cantonal Veterinary Office (VD2017.5). Experiments were carried out in accordance with the Swiss Animal Protection Act and the ARRIVE guidelines.

Results

In Fig. 1, we show typical *in vivo* HP ^{13}C MRS spectra from the brain of a single animal after MCAO surgery acquired 1 h post-reperfusion. The infusion of HP [$1\text{-}^{13}\text{C}$] lactate leads to labelling of the pyruvate pool as mediated by lactate dehydrogenase (LDH). [$1\text{-}^{13}\text{C}$] pyruvate is further metabolised to produce ^{13}C labelled bicarbonate; however, due to limited signal-to-noise ratio (SNR) we could only clearly identify the bicarbonate signal in the sum spectra in 9 out of the 15 animals that received HP [$1\text{-}^{13}\text{C}$] lactate. Chemical impurities at 176 ppm overlap with the expected [$1\text{-}^{13}\text{C}$] alanine peak, preventing reliable quantification or dynamic interpretation of this metabolite. Pyruvate hydrate, which represents <8% of pyruvate at physiological conditions³² (as it depended on the pH and temperature⁴⁸), was not detectable.

We quantified the AUC of the [$1\text{-}^{13}\text{C}$] lactate and [$1\text{-}^{13}\text{C}$] pyruvate signals to obtain the typical metabolic time course (Fig. 2). We observed larger [$1\text{-}^{13}\text{C}$] pyruvate signals in 1 h post-reperfusion injected animals compared to 2 h post-reperfusion and sham (Fig. 2). 37.5 s after the beginning of HP [$1\text{-}^{13}\text{C}$] lactate infusion, we barely detected pyruvate signals, and so we calculated pyruvate-to-lactate ratios (PLR) and bicarbonate-to-lactate ratios (BLR) from the spectra acquired during the first 37.5 s of the experiment. The corresponding anatomical T_{2W} images presented at the bottom of each time course illustrate that at 1 h post-reperfusion slight morphological modifications can be depicted, whereas 2 h post-reperfusion the characteristic striatal lesion following MCAO is readily visible. As expected, images of sham animals show no lesion.

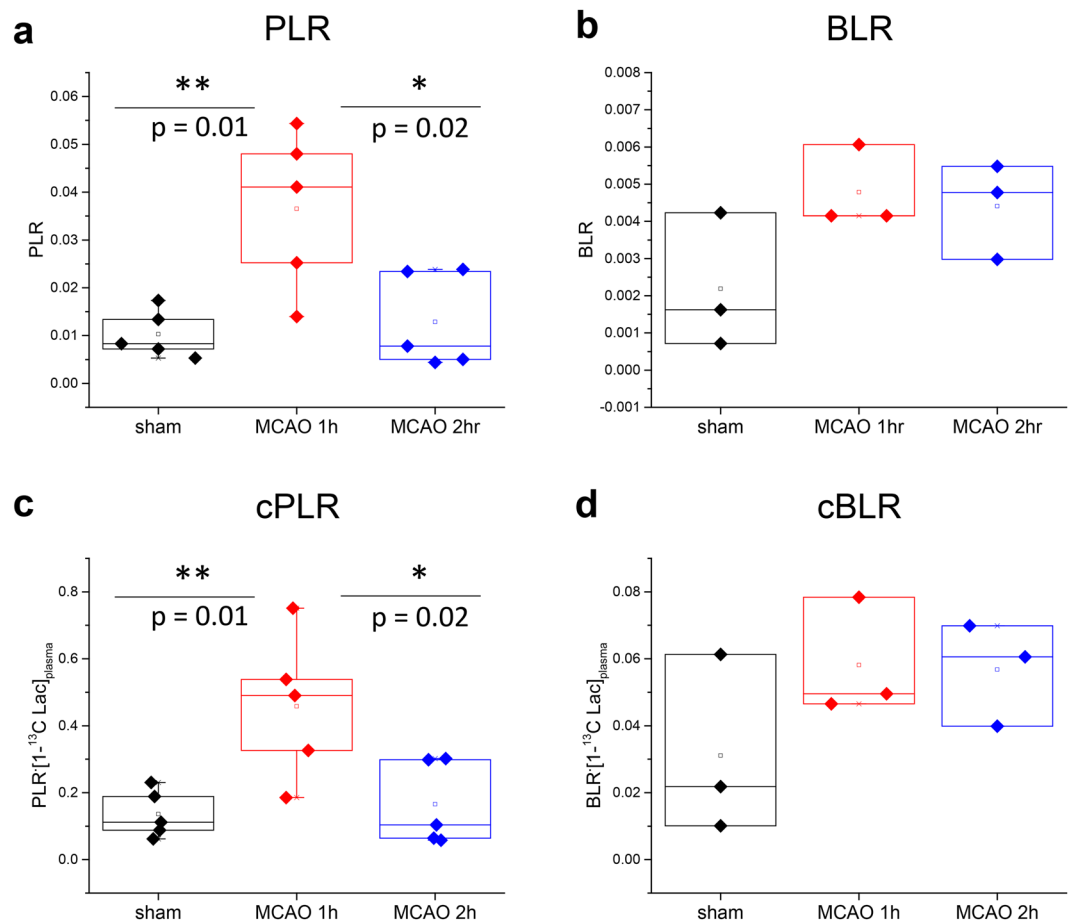


Figure 3. (a,c) Pyruvate-to-lactate ratios (PLR) and ratios corrected for $[1-^{13}\text{C}]$ lactate concentration in blood at the time of injection (cPLR), overlaid with individual data points. One-way ANOVA test indicates significant statistical difference ($p < 0.05$) between both PLR and cPLR 1 h post-reperfusion (red) and sham (black) and 2 h post-reperfusion (blue). The average values for cPLR were 0.46 ± 0.21 , 0.17 ± 0.12 and 0.14 ± 0.07 in MCAO mice 1 h and 2 h post-reperfusion and sham respectively. (b,d) Bicarbonate-to-lactate ratios (BLR) and ratios corrected for $[1-^{13}\text{C}]$ lactate concentration in blood at the time of injection (cBLR) overlaid with individual data points showing a trend for increased BLR and cBLR in MCAO mice 1 h (red) and 2 h post-reperfusion (blue) compared to sham (black). The average values for cBLR were 0.058 ± 0.018 , 0.057 ± 0.015 and 0.031 ± 0.027 in MCAO mice 1 h and 2 h post-reperfusion and sham respectively.

PLR and cPLR were significantly higher at 1 h post-reperfusion than 2 h post-reperfusion or in sham ($p < 0.05$). A trend to larger BLR and cBLR in animals experiencing MCAO surgery compared to sham animals was observed, however, no significant differences were found between the groups (Fig. 3).

Representative proton spectra acquired in the striatum of sham operated and MCAO operated mice 1 h and 2 h post-reperfusion together with the dynamic evolution of several brain metabolites showing changes compared to baseline values⁴⁹ in the first 200 minutes post-reperfusion are presented in Fig. 4. Data acquisition started as early as 20 min post-surgery in sham animals and 40 min post-reperfusion in MCAO mice. The ischaemic insult led to a large increase in lactate concentrations that reached a maximum value between 60 and 120 min post-reperfusion and then steadily decreased (Fig. 4d). The putative osmoregulator taurine (Tau) steadily decreased (Fig. 4e). Alanine (Ala) concentrations steadily increased in MCAO mice and steadily decreased in sham mice (Fig. 4f). These changes show similar trends to those reported in MCAO occluded mice 180 min post-reperfusion²⁰. The concentration of other metabolites quantified by the LC-model as well as the direction of significant changes are presented in Table 1.

In the brain, monocarboxylate transporters (MCTs) 1, 2 and 4 mediate bidirectional transport of lactate across cell membranes by diffusional, saturable symport with protons. In agreement to what has been previously reported⁴⁷, we observed changes in the distribution of MCTs after transient MCAO. Whereas in sham animals intermediate affinity MCT1 ($K_{m_{\text{lactate}}} 3.5\text{--}10\text{ mM}$, Fig. 5a) is mainly expressed in endothelial cells and brain parenchyma⁴⁶, at 1 h after reperfusion the MCT1 signal is stronger in blood vessels and in areas where neurons are still present, while it decreases in areas of neuronal loss. 2 h after reperfusion, MCT1 expression is still prominent in vessels and in surviving neurons. The high-affinity transporter MCT2 ($K_{m_{\text{lactate}}} 0.5\text{--}0.75\text{ mM}$, Fig. 5b) is expressed strongly in neurons and weakly around blood vessels in sham animals⁴⁶. At 1 h post-reperfusion and even more intensely at 2 h post-reperfusion, we observe enhanced expression of MCT2 around blood vessels. The

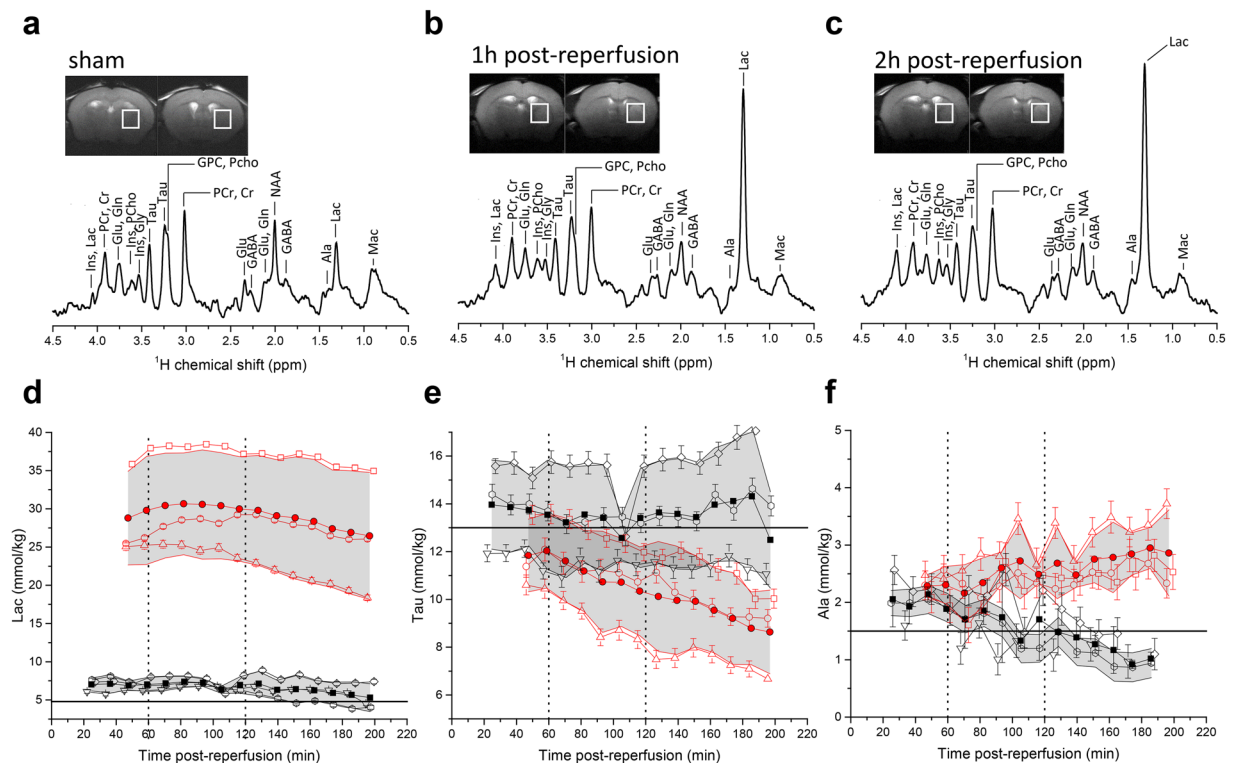


Figure 4. (a–c) Representative ¹H spectra and voxel position in the striatum of sham mice and MCAO mice 1 h and 2 h post-reperfusion. (d–f) Time course of selected metabolites after 30 min MCAO surgery (red) and sham operated mice (black); time zero indicates the beginning of reperfusion. Open symbols are individual animals, with Cramer-Rao lower bounds (CRLB) of the LC-model quantification as error bars. Full red circles are the average of all three MCAO animals and full black squares are the average of all three shams -with the grey area representing the corresponding standard deviation. Horizontal lines that designate the metabolite concentration in healthy 8-week C57BL/6J mice as reported by Tkac *et al.*⁴⁹ were added to guide the eye on the dynamic evolution of the metabolite concentrations. Vertical lines indicate the times at which HP lactate was injected in the HP ¹³C MRS measurements.

MCT2 signal is decreased in damaged areas of the striatum at both time-points, possibly due to the neuronal loss. The low-affinity, mostly astrocytic, lactate transporter MCT4 ($K_{m_{lactate}}$ 22–28 mM Fig. 5c)⁵⁰ is distributed unevenly in the striatum of sham mice, with some patches of intense expression. Similar to MCT1 and MCT2, there is an overall decrease in expression of MCT4 in areas of neuronal loss, both 1 h and 2 h post-reperfusion. Especially 2 h after reperfusion, we observe MCT4 staining in small blood vessels in the lesion areas. The patches of stronger MCT4 signal observed in sham mice are still present 1 h and 2 h post-reperfusion. Changes in MCTs expression and distribution extend to the contralateral hemisphere, where they show similar patterns to those observed in areas of the ipsilateral side with surviving neurons.

Discussion

This study demonstrates the feasibility of measuring in real-time *in vivo* metabolism of the neuroprotective agent [1-¹³C] lactate, administered at a therapeutic dose after a transient focal cerebral ischaemia using HP ¹³C MRS. We detected LDH mediated transfer⁵¹ of the ¹³C label from [1-¹³C] lactate to [1-¹³C] pyruvate, which is further transferred to ¹³C bicarbonate via PDH activity. We found a significantly higher cPLR at 1 h post-reperfusion compared to both 2 h post-reperfusion and sham animals. In addition, we observed a trend towards a higher cBLR in animals after MCAO surgery compared to sham animals, indicating that pyruvate is driven towards the TCA cycle to be metabolised (Fig. 3). Similar differences were observed for the uncorrected ratios. These findings imply that the ratios depend on the time elapsed between ischaemia onset and the beginning of reperfusion, probably reflecting the evolving metabolic reprogramming and energetic demands after the ischemic insult. Our global measurement of the entire brain indicates a significant difference in the cerebral metabolism of the exogenous HP [1-¹³C] lactate, however, at this stage we cannot identify whether it is arising from the lesion, penumbra, or remote brain area. A further step will be to localise the cPLR signals, for instance by imaging techniques, thereby mapping where the metabolic conversions take place, to understand the underlying metabolic condition of tissue in ischaemia. The SNR obtained with our current set up and HP sample formulation (in particular the chosen free radical) is too limited to perform signal localisation at a relevant spatial resolution. Improved SNR and localisation could then lead to the use of HP [1-¹³C] lactate as a molecular imaging biosensor in ischaemic stroke patients after endovascular clot removal, keeping in mind that lactate is known to improve the neurological outcome in preclinical studies¹⁵.

metabolites	Sham (3)	~ 1-h (3)	Changes at ~1-h	~2-h (3)	Changes at ~2-h
Ala	2.0 ± 0.5	2.3 ± 0.3		2.6 ± 0.5	
Cr	4.5 ± 0.2	4.5 ± 0.2		4.2 ± 0.3	
PCr	4.3 ± 0.2	2.9 ± 0.5	↓ **	2.9 ± 0.4	↓ **
Cr+PCr	8.8 ± 0.3	7.4 ± 0.5	↓ *	7.2 ± 0.6	↓ **
PCr/Cr	0.95 ± 0.06	0.64 ± 0.12	↓ **	0.70 ± 0.07	↓ *
GABA	2.3 ± 0.2	3.4 ± 0.1	↑ **	3.2 ± 0.5	↑ *
Gln	3.1 ± 0.3	3.1 ± 0.3		3.0 ± 0.6	
Glu	7.0 ± 0.3	4.8 ± 0.6	↓ ***	4.2 ± 0.2	↓ ****
Glu+Gln	10.1 ± 0.4	8.0 ± 0.9	↓ *	7.2 ± 0.7	↓ ***
Gln/Glu	0.44 ± 0.04	0.65 ± 0.01	↑ p = 0.06	0.70 ± 0.15	↑ *
GSH	1.5 ± 0.3	1.3 ± 0.5		0.9 ± 0.3	
Gly	1.6 ± 0.3	2.4 ± 0.5		2.2 ± 0.4	
myo-Ins	5.9 ± 0.3	5.0 ± 0.6		4.3 ± 0.8	↓ *
Myo-Ino + Gly	7.4 ± 0.3	7.4 ± 0.1		6.5 ± 0.7	↓ p = 0.08
Lac	7.0 ± 0.8	29.2 ± 6.9	↑ ***	28.9 ± 6.8	↑ ***
NAA	6.7 ± 0.4	4.1 ± 0.4	↓ ****	3.8 ± 0.5	↓ ****
NAA + NAAG	6.9 ± 0.4	4.1 ± 0.3	↓ ****	3.9 ± 0.5	↓ ****
Tau	14.0 ± 1.9	11.6 ± 1.9		9.8 ± 2.3	
PE	2.9 ± 0.6	1.5 ± 0.2	↓ *	1.3 ± 0.4	↓ **
Mac	1.9 ± 0.1	1.2 ± 0.1	↓ ***	1.2 ± 0.1	↓ ****
GPC + PCho	1.10 ± 0.04	1.12 ± 0.18		1.03 ± 0.25	

Table 1. Neurochemical profiles in the striatum of sham operated mice and after 30 min of transient ischaemia. Ala, alanine; Cr, creatine, PCr, phosphocreatine; GABA, γ -aminobutyric acid; Gln, glutamine; Glu, glutamate; GSH, glutathione; Gly, glycine; *myo*-Ins, myo-inositol; Lac, lactate; NAA, N-acetyl-aspartate; NAAG, N-acetyl-aspartate-glutamate; Tau, taurine; PE, phosphatidylethanolamine; Mac, macromolecule; GPC, glycerophosphocholine; PCho, phosphocholine. All concentrations, except ratios, are in mmol/kg. Number of animals is indicated in parentheses. Only metabolites with CRLB of less than 45% in all animals are presented. The changes are calculated compared to sham and displayed with specific oriented arrows (‘↓’ as decrease and ‘↑’ as increase). The number of ‘*’ represent statistically significant levels of $p = 0.05, 0.02, 0.01$ and 0.001 .

The neurochemical profiles of the ischaemic lesion area quantified from the ^1H MRS spectra and their evolution after insult at the two HP [$1\text{-}^{13}\text{C}$] lactate injection time points tested (i.e. 1 h and 2 h post-reperfusion) indicate differences in metabolite concentrations and, thus, suggest a change in the metabolic demand of the tissue at the two time points. Endogenous lactate concentrations at both 1 h and 2 h post-reperfusion were extremely elevated compared to sham and showed similar average concentrations. However, at 1 h post-reperfusion, the lactate concentration is nearly at its maximum value, while at 2 h post-reperfusion, lactate concentration is decreasing, indicating that endogenous lactate is either being consumed by the tissue or eliminated. This difference suggesting a shift in the metabolic dynamics of lactate at 1 h and 2 h may be related to the dissimilarity in response to the HP [$1\text{-}^{13}\text{C}$] lactate bolus. Interestingly, previous findings from our lab have shown divergence in the neuroprotective effect of lactate when administered at different time points after stroke¹⁵. Lactate administered 1 h after ischaemia onset (and immediately post-reperfusion) decreased lesion size and ameliorated the neurological outcome. However, administration 2 h after onset (i.e. 1 h post-reperfusion) had no effect on the lesion size, but a stronger improvement in neurological outcome.

It is important to highlight that ^1H MRS spectra were collected in a single voxel located within the striatal lesion, while the HP ^{13}C MRS, following the bolus of [$1\text{-}^{13}\text{C}$] lactate was detected over the entire brain. To better investigate the relationship between the neurochemical profile and the metabolic response to the HP [$1\text{-}^{13}\text{C}$] lactate injection, it will be of high interest to improve the sensitivity of the HP [$1\text{-}^{13}\text{C}$] lactate experiment to enhance the spatial resolution in order to localise and delimit the observed effect. Further improvement in the HP sample formulation, for instance using more efficient polarising agents (e.g. trityl), would allow enhancement of the initial polarisation level of injected [$1\text{-}^{13}\text{C}$] lactate, and therefore increase the SNR of the entire measurement, in particular for detecting [^{13}C] bicarbonate. Moreover, higher sensitivity would potentially enable us to quantify the kinetics of the transfer of the ^{13}C labelling from HP [$1\text{-}^{13}\text{C}$] lactate to other metabolites through biochemical reactions.

For the cerebral conversion of HP [$1\text{-}^{13}\text{C}$] lactate, the substrate must first cross the BBB via MCTs before being converted to [$1\text{-}^{13}\text{C}$] pyruvate by the LDH enzyme. It has been reported that in the healthy brain the BBB limits the observation of cerebral metabolism of HP monocarboxylic acids^{34,52–54}, and that the transfer of the label to pyruvate is directly related to the endogenous pool size⁵¹. We found that at the HP [$1\text{-}^{13}\text{C}$] lactate injection time points MCTs expression and distribution were altered in both brain hemispheres. MCT1, MCT2 and MCT4 expression was increased in blood vessels and MCT1 and MCT4 expression was increased in living neurons, perhaps enabling more lactate to be globally delivered to the tissue and resulting in a larger concentration of HP [$1\text{-}^{13}\text{C}$] lactate in the brain compartment that is rapidly exchanged to [$1\text{-}^{13}\text{C}$] pyruvate in cells with high energetic

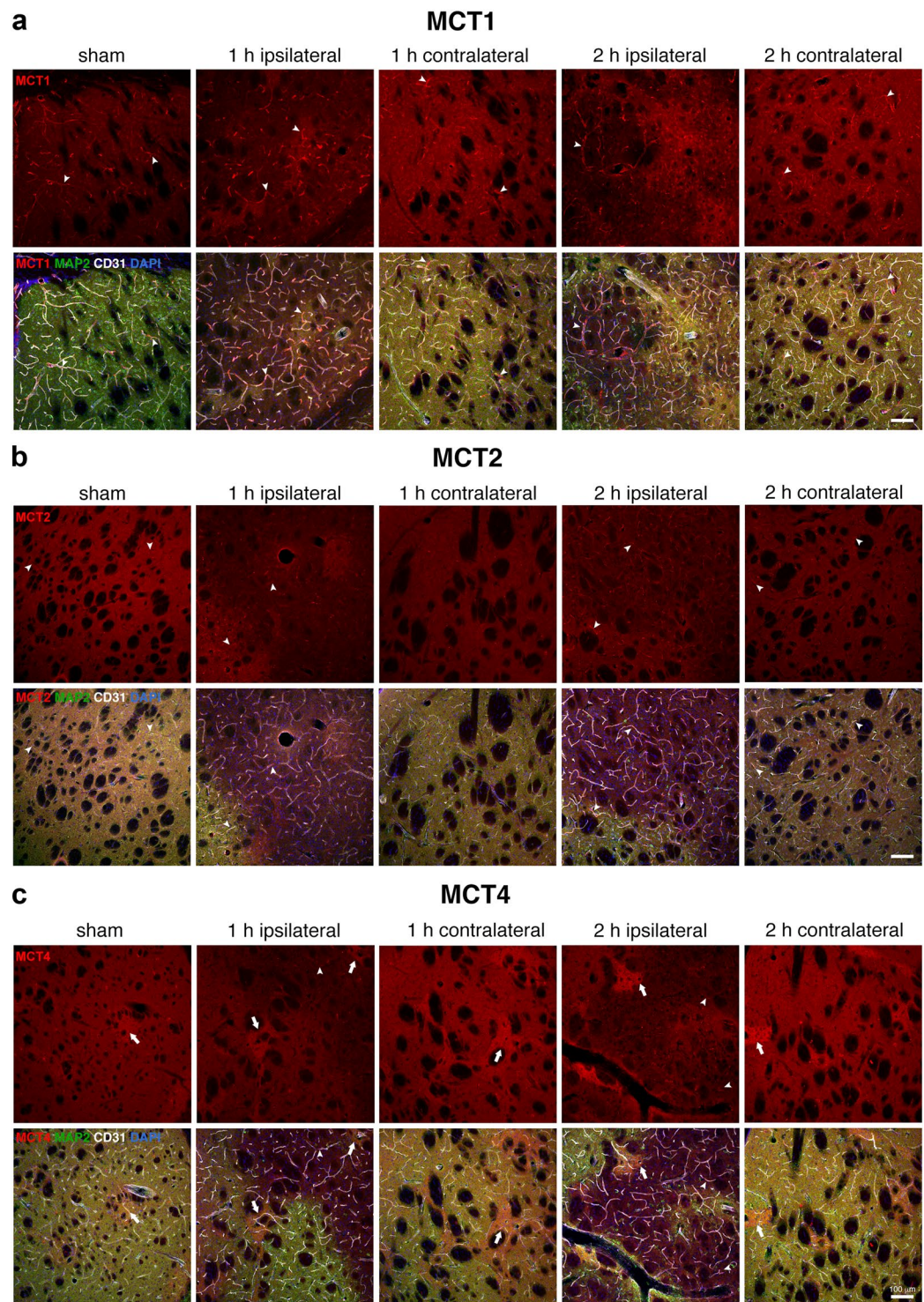


Figure 5. Changes in MCT expression patterns after ischaemia-reperfusion. The images in red in the upper panels show the expression of lactate transporters MCT1 (a), MCT2 (b) and MCT4 (c) in the striatum of sham animals and in the striatum ipsilateral and contralateral to the lesion of MCAO mice at 1 h or 2 h post-reperfusion. The lower panels show the merged images of the triple immunolabelling of the MCTs (red) with the neuronal marker MAP-2 (green) to identify the lesion area (i.e. loss of MAP-2 staining), the endothelial cell marker CD31 to identify blood vessels (grey) and the nuclear counterstaining (DAPI, blue). Arrowheads indicate blood vessels. Arrows in (c) indicate patches of high MCT4 expression. Scalebar: 100 μ m.

demand. This might be the dominant effect at 1 h post-reperfusion. However, the difference in the response to the [1- 13 C] lactate bolus 1 h and 2 h post-reperfusion is probably related to changes in lactate metabolism, as suggested by the differences in the neurochemical profiles. Further investigations are necessary to clarify the mechanisms in our system.

In this proof-of-concept study, we demonstrate the metabolism of exogenous HP [$1-^{13}\text{C}$] lactate in the mouse brain in real time and *in vivo* after transient cerebral ischaemia and its relation to the time elapsed after reperfusion. The mouse transient MCAO with suture withdrawal at the end of the ischaemia is a realistic model of the clinical situation with intervention of clot removal. HP [$1-^{13}\text{C}$] lactate has potential as a new molecular imaging biosensor after stroke, similar to HP [$1-^{13}\text{C}$] pyruvate to characterise the damage as well as differences between the penumbra, necrotic core lesion and intact regions³¹. In addition, as lactate was shown to improve neurological outcome, administration could contribute to a better post-ischaemic recovery^{15,16,18}. Moreover, further application of ^{13}C MRS of HP lactate to study cerebral metabolism in the intact brain and in MCAO animal models may help clarify the mechanism of lactate neuroprotection and elucidate lactate's proposed dual mode of action as energetic substrate and signalling agent¹⁷.

Conclusion

HP [$1-^{13}\text{C}$] lactate metabolism can be measured in a transient MCAO mouse stroke model after i.v. injection: injected lactate reaches the brain very rapidly and gets converted into pyruvate and CO_2 . Global HP ^{13}C MRS measurements demonstrate time-dependent lactate metabolism in the first two hours after reperfusion, suggesting modification in the transport and/or cerebral metabolism.

Data availability

All data is available from the authors upon reasonable request.

Received: 20 October 2019; Accepted: 5 March 2020;

Published online: 26 March 2020

References

- Johnson, W., Onuma, O., Owolabi, M. & Sachdev, S. Stroke: a global response is needed. *Bulletin of the World Health Organization* **94**, 634–634A, <https://doi.org/10.2471/BLT.16.181636> (2016).
- Campbell, B. C. *et al.* Endovascular therapy for ischemic stroke with perfusion-imaging selection. *The New England journal of medicine* **372**, 1009–1018, <https://doi.org/10.1056/NEJMoa1414792> (2015).
- Sandercock, P. *et al.* The benefits and harms of intravenous thrombolysis with recombinant tissue plasminogen activator within 6 h of acute ischaemic stroke (the third international stroke trial [IST-3]): a randomised controlled trial. *Lancet* **379**, 2352–2363, [https://doi.org/10.1016/S0140-6736\(12\)60768-5](https://doi.org/10.1016/S0140-6736(12)60768-5) (2012).
- Saver, J. L. *et al.* Time to Treatment With Endovascular Thrombectomy and Outcomes From Ischemic Stroke: A Meta-analysis. *Jama* **316**, 1279–1288, <https://doi.org/10.1001/jama.2016.13647> (2016).
- Thomalla, G. & Gerloff, C. Acute imaging for evidence-based treatment of ischemic stroke. *Current opinion in neurology* <https://doi.org/10.1097/WCO.0000000000000716> (2019).
- Stankowski, J. N. & Gupta, R. Therapeutic targets for neuroprotection in acute ischemic stroke: lost in translation? *Antioxidants & redox signaling* **14**, 1841–1851, <https://doi.org/10.1089/ars.2010.3292> (2011).
- Young, B. O. Neuroprotective strategies for acute ischemic stroke: recent progress and future perspectives. *Precision and Future. Medicine* **1**, 115–121, <https://doi.org/10.23838/pfm.2017.00149> (2017).
- Higuchi, T. *et al.* Mapping of lactate and N-acetyl-L-aspartate predicts infarction during acute focal ischemia: *in vivo* ^1H magnetic resonance spectroscopy in rats. *Neurosurgery* **38**, 121–129; discussion 129–130 (1996).
- Henriksen, O. *et al.* Cerebral lactate production and blood flow in acute stroke. *Journal of magnetic resonance imaging: JMIR* **2**, 511–517 (1992).
- Schurr, A., West, C. A. & Rigor, B. M. Lactate-supported synaptic function in the rat hippocampal slice preparation. *Science* **240**, 1326–1328 (1988).
- Schurr, A. Lactate: the ultimate cerebral oxidative energy substrate? *Journal of cerebral blood flow and metabolism: official journal of the International Society of Cerebral Blood Flow and Metabolism* **26**, 142–152, <https://doi.org/10.1038/sj.jcbfm.9600174> (2006).
- Phillis, J. W., Song, D., Guyot, L. L. & O'Regan, M. H. Lactate reduces amino acid release and fuels recovery of function in the ischemic brain. *Neuroscience letters* **272**, 195–198 (1999).
- Ros, J., Pecinska, N., Alessandri, B., Landolt, H. & Fillenz, M. Lactate reduces glutamate-induced neurotoxicity in rat cortex. *Journal of neuroscience research* **66**, 790–794, <https://doi.org/10.1002/jnr.10043> (2001).
- Schurr, A., Payne, R. S., Miller, J. J., Tseng, M. T. & Rigor, B. M. Blockade of lactate transport exacerbates delayed neuronal damage in a rat model of cerebral ischemia. *Brain research* **895**, 268–272 (2001).
- Berthet, C. *et al.* Neuroprotective role of lactate after cerebral ischemia. *Journal of cerebral blood flow and metabolism: official journal of the International Society of Cerebral Blood Flow and Metabolism* **29**, 1780–1789, <https://doi.org/10.1038/jcbfm.2009.97> (2009).
- Berthet, C., Castillo, X., Magistretti, P. J. & Hirt, L. New evidence of neuroprotection by lactate after transient focal cerebral ischaemia: extended benefit after intracerebroventricular injection and efficacy of intravenous administration. *Cerebrovascular diseases* **34**, 329–335, <https://doi.org/10.1159/000343657> (2012).
- Castillo, X. *et al.* A probable dual mode of action for both L- and D-lactate neuroprotection in cerebral ischemia. *Journal of cerebral blood flow and metabolism: official journal of the International Society of Cerebral Blood Flow and Metabolism* **35**, 1561–1569, <https://doi.org/10.1038/jcbfm.2015.115> (2015).
- Ichai, C. *et al.* Sodium lactate versus mannitol in the treatment of intracranial hypertensive episodes in severe traumatic brain-injured patients. *Intensive care medicine* **35**, 471–479, <https://doi.org/10.1007/s00134-008-1283-5> (2009).
- Carteron, L. *et al.* Hypertonic Lactate to Improve Cerebral Perfusion and Glucose Availability After Acute Brain Injury. *Critical care medicine* **46**, 1649–1655, <https://doi.org/10.1097/ccm.0000000000003274> (2018).
- Lei, H., Berthet, C., Hirt, L. & Gruetter, R. Evolution of the neurochemical profile after transient focal cerebral ischemia in the mouse brain. *Journal of cerebral blood flow and metabolism: official journal of the International Society of Cerebral Blood Flow and Metabolism* **29**, 811–819, <https://doi.org/10.1038/jcbfm.2009.8> (2009).
- Figlewski, K. *et al.* Decreased GABA levels in the symptomatic hemisphere in patients with transient ischemic attack. *Heliyon* **4**, e00790, <https://doi.org/10.1016/j.heliyon.2018.e00790> (2018).
- Ardenkjaer-Larsen, J. H. *et al.* Increase in signal-to-noise ratio of > 10,000 times in liquid-state NMR. *Proceedings of the National Academy of Sciences of the United States of America* **100**, 10158–10163 (2003).
- Mishkovsky, M. & Comment, A. Hyperpolarized MRS: New tool to study real-time brain function and metabolism. *Analytical biochemistry* **529**, 270–277, <https://doi.org/10.1016/j.ab.2016.09.020> (2017).
- Mishkovsky, M. *et al.* Measuring glucose cerebral metabolism in the healthy mouse using hyperpolarized (^{13}C) magnetic resonance. *Scientific reports* **7**, 11719, <https://doi.org/10.1038/s41598-017-12086-z> (2017).

25. Guglielmetti, C. *et al.* *In vivo* metabolic imaging of Traumatic. *Brain Injury. Scientific reports* **7**, 17525, <https://doi.org/10.1038/s41598-017-17758-4> (2017).
26. Miller, J. J. *et al.* (13)C Pyruvate Transport Across the Blood-Brain Barrier in Preclinical Hyperpolarised MRI. *Scientific reports* **8**, 15082, <https://doi.org/10.1038/s41598-018-33363-5> (2018).
27. Marjanska, M., Shestov, A. A., Deelchand, D. K., Kittelson, E. & Henry, P. G. Brain metabolism under different anesthetic conditions using hyperpolarized [1-(13)C]pyruvate and [2-(13)C]pyruvate. *NMR in biomedicine* **31**, e4012, <https://doi.org/10.1002/nbm.4012> (2018).
28. Miloushev, V. Z. *et al.* Metabolic Imaging of the Human Brain with Hyperpolarized (13)C Pyruvate Demonstrates (13)C Lactate Production in Brain Tumor Patients. *Cancer research* **78**, 3755–3760, <https://doi.org/10.1158/0008-5472.CAN-18-0221> (2018).
29. Gordon, J. W. *et al.* Translation of Carbon-13 EPI for hyperpolarized MR molecular imaging of prostate and brain cancer patients. *Magnetic resonance in medicine* <https://doi.org/10.1002/mrm.27549> (2018).
30. Grist, J. T. *et al.* Quantifying normal human brain metabolism using hyperpolarized [1-(13)C]pyruvate and magnetic resonance imaging. *NeuroImage* **189**, 171–179, <https://doi.org/10.1016/j.neuroimage.2019.01.027> (2019).
31. Xu, Y. *et al.* Hyperpolarized (13)C Hyperpolarized 13C Magnetic Resonance Imaging Can Detect Metabolic Changes Characteristic of Penumbra in Ischemic Stroke. *Tomography* **3**, 67–73, <https://doi.org/10.18383/j.tom.2017.00106> (2017).
32. Keshari, K. R. & Wilson, D. M. Chemistry and biochemistry of 13C hyperpolarized magnetic resonance using dynamic nuclear polarization. *Chemical Society reviews* **43**, 1627–1659, <https://doi.org/10.1039/c3cs60124b> (2014).
33. Chen, A. P. *et al.* Feasibility of using hyperpolarized [1-13C]lactate as a substrate for *in vivo* metabolic 13C MRSI studies. *Magnetic resonance imaging* **26**, 721–726, <https://doi.org/10.1016/j.mri.2008.01.002> (2008).
34. Takado, Y. *et al.* Hyperpolarized (13)C Magnetic Resonance Spectroscopy Reveals the Rate-Limiting Role of the Blood-Brain Barrier in the Cerebral Uptake and Metabolism of l-Lactate *In Vivo*. *ACS chemical neuroscience*, <https://doi.org/10.1021/acscchemneuro.8b00066> (2018).
35. Bastiaansen, J. A. M., Yoshihara, H. A. I., Takado, Y. & Gruetter, R. & Comment, A. Hyperpolarized C-13 lactate as a substrate for *in vivo* metabolic studies in skeletal muscle. *Metabolomics* **10**, 986–994, <https://doi.org/10.1007/s11306-014-0630-5> (2014).
36. Mayer, D. *et al.* Application of hyperpolarized [1-(1)(3)C]lactate for the *in vivo* investigation of cardiac metabolism. *NMR in biomedicine* **25**, 1119–1124, <https://doi.org/10.1002/nbm.2778> (2012).
37. Longa, E. Z., Weinstein, P. R., Carlson, S. & Cummins, R. Reversible middle cerebral artery occlusion without craniectomy in rats. *Stroke* **20**, 84–91 (1989).
38. Cheng, T., Capozzi, A., Takado, Y. & Balzan, R. & Comment, A. Over 35% liquid-state 13C polarization obtained via dissolution dynamic nuclear polarization at 7 T and 1 K using ubiquitous nitroxyl radicals. *Physical chemistry chemical physics: PCCP* **15**, 20819–20822, <https://doi.org/10.1039/c3cp53022a> (2013).
39. Comment, A. *et al.* Design and performance of a DNP prepolarizer coupled to a rodent MRI scanner. *Concept Magn Reson B* **31B**, 255–269, <https://doi.org/10.1002/cmrb.20099> (2007).
40. Cheng, T. *et al.* Automated transfer and injection of hyperpolarized molecules with polarization measurement prior to *in vivo* NMR. *NMR in biomedicine* **26**, 1582–1588, <https://doi.org/10.1002/nbm.2993> (2013).
41. Gruetter, R. & Tkac, I. Field mapping without reference scan using asymmetric echo-planar techniques. *Magnetic resonance in medicine* **43**, 319–323, [10.1002/\(SICI\)1522-2594\(200002\)43:2<319::AID-MRM22>3.0.CO;2-1](https://doi.org/10.1002/(SICI)1522-2594(200002)43:2<319::AID-MRM22>3.0.CO;2-1) [pii] (2000).
42. Staewen, R. S. *et al.* 3-D FLASH imaging using a single surface coil and a new adiabatic pulse, BIR-4. *Investigative radiology* **25**, 559–567 (1990).
43. Hau, J. & Schapiro, S. J. In *Handbook of Laboratory Animal Science, Volume I: Essential Principles and Practices* (CRC Press Taylor & Francis Group, 2010).
44. Mlynarik, V., Gambarota, G., Frenkel, H. & Gruetter, R. Localized short-echo-time proton MR spectroscopy with full signal-intensity acquisition. *Magnetic resonance in medicine* **56**, 965–970, <https://doi.org/10.1002/mrm.21043> (2006).
45. Provencher, S. W. Estimation of metabolite concentrations from localized *in vivo* proton NMR spectra. *Magnetic resonance in medicine* **30**, 672–679 (1993).
46. Pierre, K., Pellerin, L., Debernardi, R., Riederer, B. M. & Magistretti, P. J. Cell-specific localization of monocarboxylate transporters, MCT1 and MCT2, in the adult mouse brain revealed by double immunohistochemical labeling and confocal microscopy. *Neuroscience* **100**, 617–627, [https://doi.org/10.1016/s0306-4522\(00\)00294-3](https://doi.org/10.1016/s0306-4522(00)00294-3) (2000).
47. Rosafio, K., Castillo, X., Hirt, L. & Pellerin, L. Cell-specific modulation of monocarboxylate transporter expression contributes to the metabolic reprogramming taking place following cerebral ischemia. *Neuroscience* **317**, 108–120, <https://doi.org/10.1016/j.neuroscience.2015.12.052> (2016).
48. Pocker, Y., Meany, J. E., Nist, B. J. & Zadorojny, C. Reversible Hydration of Pyruvic Acid.I. Equilibrium Studies. *J Phys Chem-Us* **73**, 2879–+, <https://doi.org/10.1021/j100843a015> (1969).
49. Tkac, I. *et al.* Highly resolved *in vivo* 1H NMR spectroscopy of the mouse brain at 9.4 T. *Magnetic resonance in medicine* **52**, 478–484, <https://doi.org/10.1002/mrm.20184> (2004).
50. Pellerin, L., Bergersen, L. H., Halestrap, A. P. & Pierre, K. Cellular and subcellular distribution of monocarboxylate transporters in cultured brain cells and in the adult brain. *Journal of neuroscience research* **79**, 55–64, <https://doi.org/10.1002/jnr.20307> (2005).
51. Kennedy, B. W., Kettunen, M. I., Hu, D. E. & Brindle, K. M. Probing lactate dehydrogenase activity in tumors by measuring hydrogen/deuterium exchange in hyperpolarized l-[1-(13)C,U-(2)H]lactate. *Journal of the American Chemical Society* **134**, 4969–4977, <https://doi.org/10.1021/ja300222e> (2012).
52. Hurd, R. E. *et al.* Metabolic imaging in the anesthetized rat brain using hyperpolarized [1-13C] pyruvate and [1-13C] ethyl pyruvate. *Magnetic resonance in medicine* **63**, 1137–1143, <https://doi.org/10.1002/mrm.22364> (2010).
53. Hurd, R. E. *et al.* Cerebral dynamics and metabolism of hyperpolarized [1-(13)C]pyruvate using time-resolved MR spectroscopic imaging. *Journal of cerebral blood flow and metabolism: official journal of the International Society of Cerebral Blood Flow and Metabolism* **30**, 1734–1741, <https://doi.org/10.1038/jcbfm.2010.93> (2010).
54. Miller, J. J. *et al.* 13C Pyruvate Transport Across the Blood-Brain Barrier in Preclinical Hyperpolarised MRI. *Scientific reports* **8**, 15082, <https://doi.org/10.1038/s41598-018-33363-5> (2018).

Acknowledgements

The authors would like to thank Prof. Rolf Gruetter and Dr. Arnaud Comment for triggering this collaborative work, Dr. Hongxia Lei, and Prof. Pierre Magistretti for fruitful discussions, Prof. Luc Pellerin for providing the anti-MCT1 and anti-MCT2 antibodies and Dr Melanie Price for proofreading the manuscript. This work was supported by the Swiss National Science Foundation (grant #310030_170155), the Centre d'Imagerie BioMédicale (CIBM) of the UNIL, UNIGE, HUG, CHUV, EPFL, and the Leenards, Jeantet, Biaggi and Juchum Foundations.

Author contributions

J.N.H., L.B., T.P.L., M.L. and M.M. generated the data; L.H., M.M., J.N.H., L.B. contributed to the experimental design and analysis; J.N.H., L.B., T.P.L., M.L., L.H. and M.M. took part in writing the manuscript.

Competing interests

The authors declare no competing interests.

Additional information

Supplementary information is available for this paper at <https://doi.org/10.1038/s41598-020-62319-x>.

Correspondence and requests for materials should be addressed to M.M.

Reprints and permissions information is available at www.nature.com/reprints.

Publisher's note Springer Nature remains neutral with regard to jurisdictional claims in published maps and institutional affiliations.



Open Access This article is licensed under a Creative Commons Attribution 4.0 International License, which permits use, sharing, adaptation, distribution and reproduction in any medium or format, as long as you give appropriate credit to the original author(s) and the source, provide a link to the Creative Commons license, and indicate if changes were made. The images or other third party material in this article are included in the article's Creative Commons license, unless indicated otherwise in a credit line to the material. If material is not included in the article's Creative Commons license and your intended use is not permitted by statutory regulation or exceeds the permitted use, you will need to obtain permission directly from the copyright holder. To view a copy of this license, visit <http://creativecommons.org/licenses/by/4.0/>.

© The Author(s) 2020